Received: 18 August 2023 | Revised: 4 September 2023 | Accepted: 22 August 2023

DOI: 10.1096/fba.2023-00084

RESEARCH ARTICLE

FASEB BioAdvances WILEY

Progranulin deficiency exacerbates cardiac remodeling after myocardial infarction

Takahiro Sasaki[1] | **Yoshiki Kuse**[1] | **Shinsuke Nakamura**[1] | **Masamitsu Shimazawa**[1,2] | **Hideaki Hara**[1,2]

[1]Molecular Pharmacology, Department of Biofunctional Evaluation, Gifu Pharmaceutical University, Gifu, Japan

[2]Laboratory of Collaborative Research for Innovative Drug Discovery, Gifu Pharmaceutical University, Gifu, Japan

Correspondence
Hideaki Hara, Molecular Pharmacology, Department of Biofunctional Evaluation, Gifu Pharmaceutical University, 1-25-4 Daigaku-nishi, Gifu 501-1196, Japan.
Email: hidehara@gifu-pu.ac.jp

Abstract

Myocardial infarction (MI) is a lethal disease that causes irreversible cardiomyocyte death and subsequent cardiovascular remodeling. We have previously shown that the administration of recombinant progranulin (PGRN) protects against myocardial ischemia and reperfusion injury. However, the post-MI role of PGRN remains unclear. In the present study, we investigated the effects of PGRN deficiency on cardiac remodeling after MI. Wild-type and PGRN-knockout mice were subjected to MI by ligation of the left coronary artery for histological, electrophysiological, and protein expression analysis. Cardiac macrophage subpopulations were analyzed by flow cytometry. Bone marrow-derived macrophages (BMDMs) were acquired and treated with LPS + IFN-γ and IL-4 to evaluate mRNA levels and phagocytic ability. PGRN expression was gradually increased in the whole heart at 1, 3, and 7 days after MI. Macrophages abundantly expressed PGRN at the border areas at 3 days post-MI. PGRN-knockout mice showed higher mortality, increased LV fibrosis, and severe arrhythmia following MI. PGRN deficiency increased the levels of CD206 and MerTK expression and macrophage infiltration in the infarcted myocardium, which was attributed to a larger subpopulation of cardiac $CCR2^{+}$ $Ly6C^{low}$ $CD11b^{+}$ macrophages. PGRN-deficient BMDMs exhibited higher TGF-β, IL-4R, and lower IL-1β, IL-10 and increased acute phagocytosis following stimulation of LPS and IFN-γ. PGRN deficiency reduced survival and increased cardiac fibrosis following MI with the induction of abnormal subpopulation of cardiac macrophages early after MI, thereby providing insight into the relationship between properly initiating cardiac repair and macrophage polarization after MI.

KEYWORDS

macrophage, myocardial infarction, progranulin

1 | INTRODUCTION

Cardiovascular diseases (CVDs) are the leading cause of death worldwide.[1] It is estimated that 17.9 million deaths are attributable to CVDs, which accounts for 32% of all deaths globally.[2] Myocardial infarction (MI) causes sudden and subsequent death and is characterized by myocardial necrosis following the occlusion of coronary arteries.[3] Although the survival rate after MI has improved with the development of reperfusion therapy, approximately one out of four patients with MI endure heart failure (HF).[4] Current drug therapies have not fully suppressed the worsening of HF after MI and further improvements to the prognosis have plateaued. Therefore, determining post-MI pathophysiology can aid in the exploration of novel therapeutic agents to ameliorate the prognosis of HF after MI.

Cardiac pathophysiology after MI consists of several phases: the inflammatory phase (first 3 days after MI), the reparative phase (days 3–14), and the maturation phase (days 14–).[5,6] Impaired transition from inflammatory to reparative phase promotes subsequent cardiovascular events and adverse cardiac remodeling, resulting in a poor prognosis. Macrophages support cardiac healing after MI through a self-regulating transitional phase from proinflammatory (M1) to reparative (M2) phenotypes.[7] CD206 is known as a marker of M2 macrophages, which generally increase from the end of the inflammatory phase.[8] Macrophages engulf and remove apoptotic cardiomyocytes via macrophage efferocytosis receptor myeloid-epithelial-reproductive tyrosine kinase (MerTK).[9] In previous reports, adverse cardiac remodeling after MI has been induced by aberrant increases in either M1 or M2 phenotypes.[10,11] Understanding the phenotypic changes in macrophages is important for appropriate cardiac repair and the prevention of HF after MI, but the pathophysiology is still unclear.

Progranulin (PGRN) is a glycoprotein consisting of 593 amino acids, which has 7.5 repeats of the motif composed of 12-cysteine residues.[12] PGRN has multiple functions associated with wound healing and immune modulation and is mainly expressed in immune cells, including macrophages and neutrophils.[13-16] Previous reports have shown that PGRN has protective effects on ischemic pathology in the brain and kidney.[17,18] We have also reported that administration of PGRN protects against cardiac injury after MI in mice and rabbits.[19] However, the role of endogenous PGRN in cardiac remodeling after MI remains unclear. PGRN has been implicated in the regulation of macrophage function and polarization. There are conflicting reports stating that PGRN-deficient macrophages severely increase either M1-like proinflammatory cytokines by LPS treatment, or CD206 expression recognized as an M2-like phenotype after cardiotoxin-induced muscle injury.[20,21] Nevertheless, the absence of PGRN appears to consistently induce an unfavorable phenotype in macrophages. Therefore, we hypothesized that PGRN deficiency causes adverse cardiac remodeling via impaired macrophage polarization after MI.

Here, we show that PGRN plays a key role in the prevention of adverse cardiac remodeling after MI through the functional regulation of macrophages. PGRN deficiency appears to impair macrophage recruitment and polarization after MI. Our findings contribute to the knowledge of the pathophysiology toward the initiation of appropriate cardiac repair following MI.

2 | METHOD

2.1 | Animals

Male adult ICR mice were purchased from Japan SLC Ltd (Hamamatsu, Japan) and used only for the experiments

FIGURE 1 Dynamic alterations of PGRN expression associated with macrophages throughout infarcted myocardium. (A) Immunoblots exhibit PGRN (58–68 kDa) and GAPDH (37 kDa) in whole hearts at 1, 3, 7, and 14 days after myocardial infarction (MI). (B) Quantitative analysis of PGRN expression level normalized to GAPDH in the entire infarcted myocardium. Data are the means ± SEM (Sham group: $n = 5$, MI groups; 1 d: $n = 6$, 3 d: $n = 6$, 7 d: $n = 5$, 14 d: $n = 6$). *$p < 0.05$, **$p < 0.01$ versus Sham group (one-way ANOVA followed by Dunnett T3 test). (C) Scheme of a myocardial transverse section after MI. The myocardium was classified into three different regions as follows: infarct, border, and remote areas. (D) Confocal microscopic images (×10 magnification) of PGRN at 3 days after MI. Scale bar: 500 μm. (E) Quantitative analysis of fluorescence intensity for PGRN at 3 days after MI. Data are the means ± SEM (Normal: $n = 5$, Sham: $n = 5$, Infarct: $n = 5$, Border: $n = 5$, Remote: $n = 5$). **$p < 0.01$ versus Sham group (one-way ANOVA followed by Dunnett T3 test). (F) Enlarged images of a cell expressing PGRN. The white arrows indicate one of the CD68+ PGRN+ cells. Scale bar: 10 μm. (G) Typical confocal microscopic images (×20 magnification) of macrophages at border areas 3 days after MI. Blue: nuclei stained with Hoechst 33342, Red: Troponin-I, Magenta: CD68, Green: PGRN. Scale bar: 100 μm. (H–J) Quantitative analysis of the number of CD86+ cells, PGRN+ CD68+ cells, and % of PGRN+ cells in CD 68+ cells at border areas 3 days after MI. Data are the means ± SEM (Sham: $n = 5$, MI: $n = 5$). **$p < 0.01$, ***$p < 0.001$ versus Sham-operated group (Levene's test followed by Student's or Welch's two-tailed t-test). (K) scRNA-seq analysis of cell clusters expressing Granulin (GRN) gene at 3 days post-MI. Data are the means ± SEM (Fibroblast lineage: $n = 262$, Endothelial & Mural: $n = 355$, Monocyte & Macrophage: $n = 3184$, Lymphoid: $n = 73$, Glial: $n = 1$). ****$p < 0.0001$ versus Monocyte & Macrophage (one-way ANOVA followed by Tuckey's test).

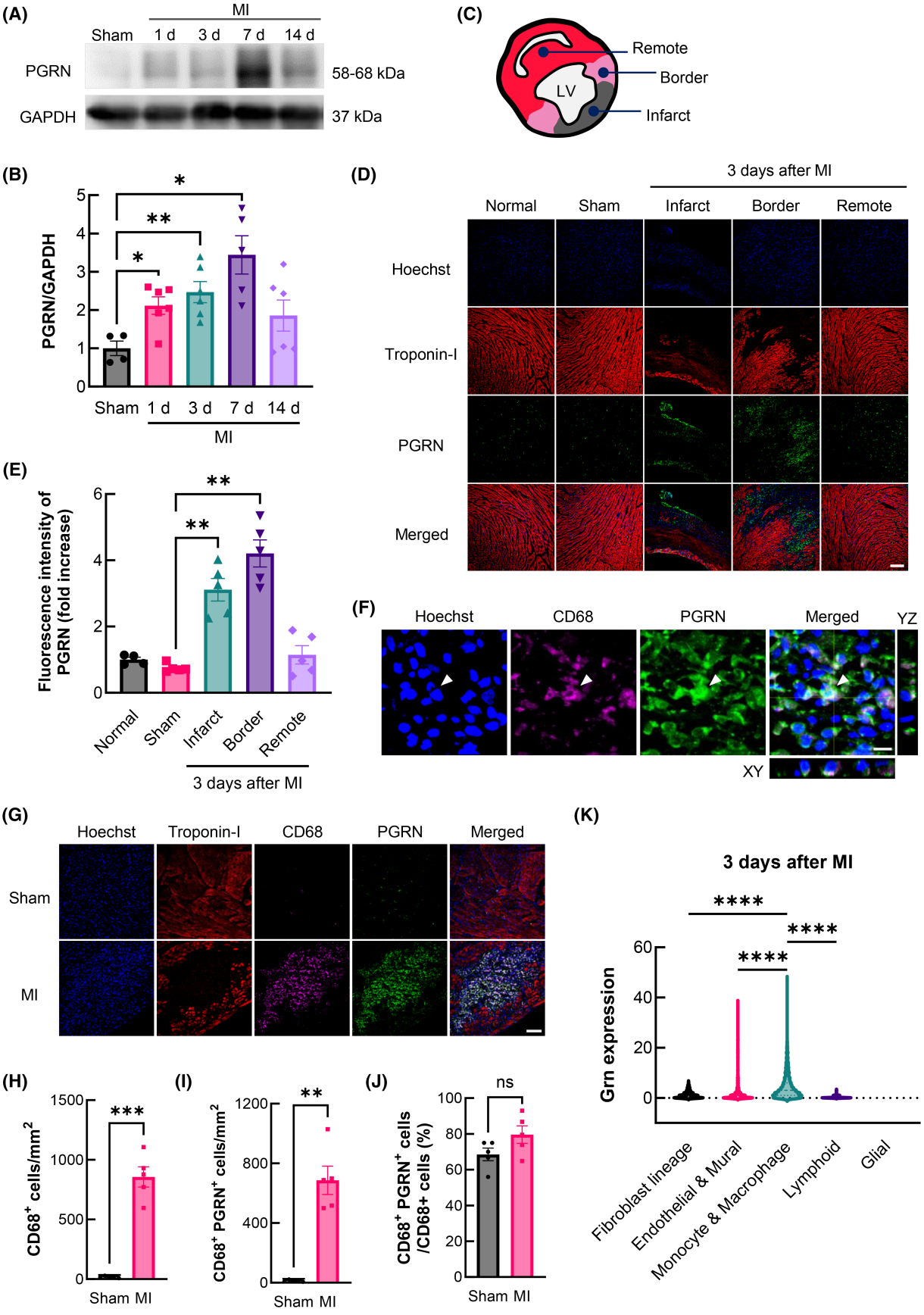
(A)
MI
Sham
1 d
3 d
7 d
14 d
PGRN
58-68 kDa
GAPDH
37 kDa
(C)
Remote
Border
LV
Infarct
(B)
PGRN/GAPDH
Sham
1 d
3 d
7 d
14 d
MI
(D)
3 days after MI
Normal
Sham
Infarct
Border
Remote
Hoechst
Troponin-I
PGRN
Merged
(E)
Fluorescence intensity of PGRN (fold increase)
Normal
Sham
Infarct
Border
Remote
3 days after MI
(F)
Hoechst
CD68
PGRN
Merged
YZ
XY
(G)
Hoechst
Troponin-I
CD68
PGRN
Merged
Sham
MI
(H)
CD68+ cells/mm2
Sham
MI
(I)
CD68+ PGRN+ cells/mm2
Sham
MI
(J)
CD68+ PGRN+ cells /CD68+ cells (%)
ns
Sham
MI
(K)
3 days after MI
Grn expression
Fibroblast lineage
Endothelial & Mural
Monocyte & Macrophage
Lymphoid
Glial

of Figure 1A–J. PGRN-knockout (PGRN-KO) mice generated by the method of Kayasuga et al. were obtained from Riken BioResource Center (Tsukuba, Japan) and were backcrossed to C57BL/6J mice.[22] Animal protocols were conducted according to the National Institutes of Health Guidelines on the Use of Laboratory Animals and were approved and monitored by the Institutional Animal Care and Use Committees and Institutional Biosafety Committees of Gifu Pharmaceutical University and Gifu University. All mice in our animal facilities were maintained at 23 ± 3°C under 12 h light–dark cycles with free access to food and water.

2.2 | Mouse MI model

Mice were subjected to MI by ligation of the left coronary artery (LCA), as described previously.[23] Briefly, mice were anesthetized with 1.0%–3.0% isoflurane in 70% N_2O and 30% O_2, delivered through a facemask using a veterinary anesthesia machine (Soft Lander; Shin-ei Industry Co., Ltd., Saitama, Japan). Mice were then endotracheally intubated with a 20-gauge plastic cannula and connected via plastic tubing to a ventilator (Model 687; Harvard Apparatus, Holliston, MA). The left thoracotomy was performed for exposure to the LCA under positive-pressure ventilation. LCA was ligated using 7–0 silk threads (alfresa, Tokyo, Japan). Successful occlusion of LCA was confirmed by regional cyanosis of the myocardial surface. The muscle layers and skin were closed using 3–0 silk sutures (Ethicon, Inc., Raritan, NJ). In sham-operated mice, the same surgical procedures were performed without ligation of LCA. Body temperature was maintained throughout the procedures using a heating pad (HEATINGPAD-2; Bioresearch Center, Co., Nagoya, Japan).

2.3 | Western blot analysis

Mice were euthanized by intraperitoneal injection of sodium pentobarbital (50 mg/kg). Isolated hearts were homogenized in lysis buffer [50 mM Tris HCl (pH 8.0), 150 mM NaCl, 0.5% sodium deoxycholate, 0.1% SDS, 1% IGEPAL CA-630, 1% Triton X-100, phosphatase inhibitor cocktail, and protease inhibitor cocktail (Sigma-Aldrich, Inc., St. Louis, MO)] using a homogenizer (NS-310EIII; Microtec Co., Ltd., Chiba, Japan). The homogenate solution was centrifuged at 10,000 rpm for 20 min at 4°C, and the protein concentration of the supernatant was measured, compared to bovine serum albumin with a bicinchoninic acid protein assay kit (Pierce Biotechnology, Inc., Waltham, MA). A mixture of equal parts protein and sample buffer with 10% 2-mercaptoethanol was separated on a 5%–20% sodium dodecyl sulfate–polyacrylamide gel electrophoresis (SDS-PAGE) gradient gel (SuperSep Ace; Wako Pure Chemical Industries, Ltd., Osaka, Japan), and the proteins were transferred to polyvinylidene difluoride membranes (Immobilon-P; Millipore Corporation, Billerica, MA). After transfer, the membranes were washed with TBS (T-TBS: 10 mM tris, 40 mM tris hydrochloride, 15 mM NaCl) containing 0.05% Tween-20 solution (TBS-T). The transferred membranes were blocked with Blocking One-P (Nacalai Tesque, Inc., Kyoto, Japan) for 30 min at room temperature and incubated with different primary antibodies at 4°C overnight. The following primary antibodies were used for immunoblotting: sheep anti-PGRN (1:1000; R&D systems Inc., Minneapolis, MN), goat anti-MerTK (1:1000; R&D systems Inc.), rabbit anti-CD206 (1:1000; Abcam, Inc., Cambridge, UK), rabbit anti-COX-2 (1:1000; Cell Signaling Technology, Danvers, MA), rabbit anti-MMP-9 (1:1000; Cell Signaling Technology), rabbit anti-phosphorylated Akt (1:1000; Cell Signaling Technology), rabbit anti-Akt (1:1000; Cell Signaling Technology), goat anti-CCL2 (1:1000; R&D systems Inc.), rabbit anti-αSMA (1:1000; Abcam, Inc.) and rabbit anti-GAPDH (1:1000; Cell Signaling Technology). After incubation of the primary antibodies, the following secondary antibodies were used: horseradish peroxidase (HRP)-conjugated goat anti-rabbit (1:2000; Pierce Biotechnology, Inc.), HRP-conjugated rabbit anti-sheep IgG (1:2000; Pierce Biotechnology, Inc.) and HRP-conjugated rabbit anti-goat IgG (1:75,000; Pierce Biotechnology, Inc.). Immunoreactive bands were visualized by Immuno Star LD (Fujifilm Wako Pure Chemical Industries, Ltd., Osaka, Japan) and Amersham Imager 680 blot and gel imager (Cytiva; Marlborough, MA).

2.4 | Immunostaining

Isolated hearts were fixed in 4% PFA for 48 h at 4°C, immersed in 25% sucrose for 24 h, and then, the hearts were embedded in an optimal cutting temperature compound (Sakura Finetechnical Co., Ltd., Tokyo, Japan). Transverse cryosections of 10 μm thickness were prepared using a cryostat vibratome (Leica CM 1850; Leica Microsystems, Inc., Wetzlar, Germany), and placed on glass slides (MAS COAT; Matsunami Glass Ind., Ltd., Osaka, Japan). The sections were blocked with 5% normal horse serum (Sigma-Aldrich, Inc.) in PBS for 1 h at room temperature, and then incubated with the primary antibodies of PGRN (1:100; R&D systems, Inc.), CD68 (1:100; Bio-Rad Laboratories Inc., Hercules, CA), Troponin-I (1:100; Abcam, Inc.), NIMP-R14 (1:100; Abcam,

Inc.) and CoraLite® 594-conjugated Cardiac Troponin-I monoclonal antibody (1:100; Proteintech, Inc., Rosemont, IL) overnight at 4°C. After incubation, the sections were washed three times with PBS for 10 min each time and incubated with the secondary antibodies of Alexa Fluor 488 donkey anti-rabbit IgG (1:1000; Molecular Probes, Eugene, OR), Alexa Fluor 546 goat anti-rat IgG (1:1000; Molecular Probes) and Alexa Fluor 647 donkey anti-sheep IgG (1:1000; Molecular Probes) for 1 h at room temperature. After washing three times with PBS, the sections were incubated in Hoechst 33342 (1:1000; Molecular Probes) for 10 min to stain nuclei. Finally, sections were mounted using a Vectashield fluorescent mounting medium (Vector Laboratory, Burlingame, CA) and cover-slipped for microscopic observation. Sections were visualized and captured digitally using a confocal microscope at 10×, 20×, and 40× magnification (Fluoview FV3000; Olympus, Tokyo, Japan). Fluorescence intensity was measured using image-processing software (Fiji-ImageJ; National Institutes of Health, Bethesda MD, USA) and shown as the average of at least three section images. The areas of infarct, border, and remote were classified as previously described.[24]

2.5 | Fibrosis size analysis

Isolated hearts were fixed in 4% PFA for 48 h at 4°C and embedded in paraffin. The embedded paraffin sections of 6 μm thickness were prepared and stained by Masson's trichrome stain kit (Sigma-Aldrich, Inc.). All images were digitally captured using a fluorescence microscope (BZ-X710; Keyence). After Masson's trichrome staining, blue areas were measured as fibrotic lesions using Fiji-ImageJ. Fibrosis size was calculated as the percentage of the total fibrotic area in the total left ventricular area of five sections from the apex to the ligature and was expressed as an average of three times.

2.6 | Infarct size analysis

Mice were euthanized with an intraperitoneal injection of sodium pentobarbital (50 mg/kg i.p.) at 24 h after ligation of LCA. The isolated heart was sliced transversely into 4 sections below the ligation site. The sections were incubated with 2% triphenyl tetrazolium chloride (TTC) in saline for 20 min at room temperature and fixed in 10% buffer formalin overnight. The slices were imaged with a digital camera (Coolpix 4500; Nikon, Tokyo, Japan). Infarct areas were measured using Fiji-ImageJ. The infarct size was calculated as a percentage of the total infarct area in the total left ventricular area.

2.7 | Electrocardiography analysis

Electrocardiography (ECG) was performed as previously described.[25,26] Briefly, mice were anesthetized with an intraperitoneal injection of a mixture of medetomidine (0.3 mg/kg), midazolam (4 mg/kg), and butorphanol (5 mg/mL). Signals were recorded at 4 kHz and filtered using a high-pass setting of 0.3 Hz and a low-pass setting of 1 kHz. Needles were inserted subcutaneously near the left hindlimb and right forelimb for lead II, and the right hindlimb for the ground electrode. During the ECG recordings, the mice were kept on a heating pad to maintain a constant body temperature. Averaged signal ECGs were generated by the complexes of time up to 60 s, and the resulting signal was analyzed manually using LabChart v8 software (ADInstruments, Dunedin, New Zealand). The isoelectric line was defined as the segment between the end of the T wave and the onset of the P wave.

2.8 | Preparation of cardiac immune cells

Cardiac immune cells were acquired as previously described.[27] Mice were euthanized by hyperesthesia with isoflurane. The heart was exposed, cut off the left and right atria, and then perfused with 10 mL of cold saline twice on each side using a 10 mL syringe fitted with an 18 G needle. The atria and major vessels were pulled off. The heart was placed on a dish, added 200 μL of Dulbecco's modified Eagle's medium (DMEM; Nacalai Tesque), and minced to a smooth consistency. The minced heart was suspended in 800 μL of DMEM, centrifuged at 50×*g* for 2 min, and thrown away the supernatant. Then, 2 mL of Hank's Balanced Salt Solution (HBSS; Nacalai Tesque) containing collagenase I (450 U/mL; Worthington biochemical Co., Vassar Avenue Lakewood, NJ, USA), hyaluronidase (60 U/mL; Sigma-Aldrich, Inc.), and DNase-I (60 U/mL; Nippon Gene Co., Ltd., Tokyo., Japan) was added and incubated at 37°C for 60 min. After incubation, a sample was vortexed for 30 s, pipetted to homogeneous suspension, and added in 12 mL of HBB buffer (HBSS, 2% FBS, 0.2% bovine serum albumin) through filtration. The suspension was centrifuged at 400×*g* for 5 min at 4°C followed by the removal of the supernatant. The pellets were hemolyzed with Red Blood Cell Lysis Buffer (Thermo Fisher Scientific, Waltham, MA, USA), resuspended by vortex, and incubated for 5 min at room temperature. The suspension was added in 5 mL of HBSS and centrifuged at 400×*g* for 5 min at 4°C. After discarding the supernatant, the pellets were resuspended in 100 μL of Cell Staining Buffer (BioLegend Co, Inc., San Diego, CA, USA).

2.9 | Flow cytometric analysis

The cell suspension was prepared at a density of 1.0×10^6 cells per 100 μL of Cell Staining Buffer. The suspension was incubated with 0.25 μg of Fc-Receptor Blocker [TruStain FcX™ PLUS (anti-mouse CD16/32) Antibody; BioLegend Co, Inc.] for 10 min followed by addition of the conjugated primary antibodies as follows: FITC anti-Ly6C antibody (1:100; BioLegend Co, Inc.), PE anti-CD11b antibody (1:100; BioLegend Co, Inc.), APC anti-CCR2 antibody (1:100; BioLegend Co, Inc.), PerCP/Cyanine5.5 anti-CD206 antibody (1:100; BioLegend Co, Inc.) and PE/Cyanine7 anti-MerTK antibody (1:100; BioLegend Co, Inc.). Twenty min after incubation, the suspension was added 2 mL of Cell Staining Buffer, and centrifuged at 400×*g* for 5 min at 4°C. The pellets were resuspended and centrifuged at 400×*g* for 5 min at 4°C. The cells were resuspended and fixed in 1 mL of 4% PFA for 20 min. The suspension was added 2 mL of Cell Staining Buffer centrifuged at 400×*g* for 5 min at 4°C, three times. The sample was analyzed by a flow cytometer and cell sorter software (Cell Sorter SH800S; Sony Co., Inc., Tokyo, Japan).

2.10 | Primary peritoneal macrophage culture

Mouse peritoneal macrophages were collected by lavage of the peritoneal cavity with 5 mL of sterile FBS-free DMEM. The cells were centrifuged and suspended in FBS-free DMEM, and the isolated cells were seeded in 24-well plates at a density of 5.0×10^4 cells/well. Thirty min after seeding, any unadhered cells were washed away with FBS-free medium, and then the cells were grown in DMEM containing 10% FBS for 24 h at 37°C, in a humidified atmosphere of 95% air and 5% CO_2 or in hypoxia (94% N_2, 5% CO_2, 1% O_2).

2.11 | Primary bone marrow-derived macrophage culture

Mice were euthanized by hyperesthesia with isoflurane. The femur and tibia were harvested, unilaterally cut, and centrifuged at 10,000 *g* for 10 s. Obtained cells were hemolyzed with Red Blood Cell Lysis Buffer for 30–60 s. The cells were suspended in 10 mL of DMEM including 10% FBS and 100 U/mL penicillin (Meiji Seika Pharma Co., Ltd., Tokyo, Japan) and 100 μg/mL streptomycin (Meiji Seika Pharma) (10% FBS DMEM), and then were centrifuged at 1300 rpm for 5 min. After resuspension, the cells were seeded at a density of 5.0×10^5 cells/mL in 12-well plates with 10% FBS DMEM including 10 ng/mL macrophage colony-stimulating factor (M-CSF; R&D Systems Minneapolis, MN, USA) and incubated under a humidified atmosphere of 5% CO2 at 37°C. The cells were incubated for 4 days with the medium changed every 2 days. Bone marrow-derived macrophages were treated with LPS (10 ng/mL) + IFN-γ (20 ng/mL) and IL-4 (20 ng/mL) for 48 h to induce M1- and M2-like macrophages.[28]

2.12 | Quantitative real-time reverse transcription polymerase chain reaction (RT-PCR) analysis

RNA was isolated from peritoneal macrophages and bone marrow-derived macrophages using Nucleo Spin RNA II (Takara Bio Inc., Shiga, Japan). RNA concentrations were measured using NanoVue Plus (GE Healthcare, Chicago, IL). Reverse transcription was performed from the isolated RNA using PrimeScript RT Reagent Kit (Perfect Real Time; Takara Bio Inc.) to synthesize single-stranded cDNA. Quantitative real-time RT-PCR was conducted using TB Green Premix ExTaq II (Tli RNaseH Plus; Takara Bio Inc.) and a TP800 Thermal Cycler Dice RealTime System (Takara Bio Inc.). All procedures were carried out

TABLE 1 Sequences of primers (mouse) used for RT-qPCR.

Gene	Forward 5′ → 3′	Reverse 5′ → 3′
CD206	CAAGGAAGGTTGGCATTTGT	CCTTTCAGTCCTTTGCAAGC
IL-1β	AACCTGCTGGTGTGTGACGTTC	CAGCACGAGGCTTTTTTGTTGT
IL-6	TCTGCAAGAGACTTCCATCCAGT	TCTGCAACTGCATCATCGTTGT
TNF-α	GAGTGACAAGCCTGTAGCC	CTCCTGGTATGAGATAGCAAA
CCL2	CTGAAGCCAGCTCTCTCTTCCT	CAGGCCCAGAAGCATGACA
IL-10	GCTCTTACTGACTGGCATGAG	CGCAGCTCTAGGAGCATGTG
IL-4Rα	TGACCTCACAGGAACCCAGGC	GAACAGGCAAAACAACGGGAT
TGF-β	CTGCTGACCCCCACTGATAC	AGCCCTGTATTCCGTCTCCT
Grn	CTGCCCGTTCTCTAAGGGTG	ATCCCCACGAACCATCAACC
β-Actin	CGA GGT GAC AGA GAC CAC AA	CTG GAG TCA AGC CAG ACA CA

according to the manufacturer's instructions. The PCR primer sequences are shown in Table 1. Cycling conditions followed the manufacturer's protocol. Specifically, 40 cycles were performed, with 5 s at 95°C and 30 s at 60°C as one cycle. The results are shown as relative gene expression levels normalized to that of β-actin.

2.13 | Phagocytosis assay

Bone marrow-derived macrophages (BMDMs) were seeded at a density of 5.0×10^4 cells/well in 96-well plates with 10% FBS DMEM including 10 ng/mL M-CSF and incubated under a humidified atmosphere of 5% CO2 at 37°C for 24 h. Then, BMDMs were treated with 50 ng/mL LPS for 1, 6, and 24 h.[29] After LPS stimulation, BMDMs were incubated with Latex beads (L3030; Sigma-Aldrich, Inc.) for 4 h, and washed three times with PBS. Fluorescence intensity was measured at excitation 575 nm and emission 610 nm by spectrophotometer (Varioskan; Thermo Electron Corporation, Vantaa, Finland). The cells were incubated with Hoechst 33342 (1:1000) for 15 min and digitally captured and counted by a fluorescence microscope (BZ-X710; Keyence). Phagocytic activity was calculated as fluorescence intensity corrected by the number of cells.

2.14 | H9c2 cell culture

Rat cardiomyocytes (H9c2) (European Collection of Authenticated Cell Culture, Wiltshire, UK) were maintained in DMEM high glucose (Sigma-Aldrich, Inc.) containing 100 units/mL penicillin, 100 μg/mL streptomycin (Meiji Co. Ltd., Tokyo, Japan) and 10% fetal bovine serum (FBS; Valeant, Costa Mesa, CA, USA) at 37°C and 5% CO_2.

2.15 | Cardiomyocyte hypertrophy

H9c2 cells were seeded at a density of 10,000 cells/well in 24-well plates with DMEM high glucose containing 10% FBS and cultured at 37°C and 5% CO_2 for 24 h. Then, the medium was replaced with DMEM 1% FBS and treated with 1 μM Angiotensin II (Ang II; Cayman Chemical Co., Ann Arbor, MI, USA), 250 ng/mL recombinant mouse PGRN (R&D systems, Inc.) and PBS for 24 h. The cells were washed with PBS and fixed in 4% PFA at room temperature for 20 min. Fixed cells were rinsed three times in PBS and immersed in phalloidin 594 conjugate working solution (1:1000; Cayman Chemical Co.) at room temperature for 60 min. The cells were washed three times with PBS, incubated with Hoechst 33342 (1:1000) for 15 min, and then imaged using a fluorescence microscope (BZ-X710; Keyence). Cell surface areas (μm^2) were measured using Fiji-ImageJ.

2.16 | Single-cell RNA sequence analysis

GRN mRNA levels were analyzed in the single cell of the heart after MI using publicly available single-cell RNA sequence (scRNA-seq) datasets with various cell populations available. These data are deposited in the ArrayExpress database at EMBL-EBI (www.ebi.ac.uk/arrayexpress) under accession codes E-MTAB-7376 and E-MTAB-7365 (Farbehi et al.). Downloaded single-cell data have already been annotated as activated fibroblasts (F-Act), fibroblast-Sca1high (F-SH), fibroblast-Sca1low (F-SL), myofibroblasts (MYO), fibroblasts expressing Wnt (F-WntX), endothelial cells (ECs), mural cells (Mural), cycling EC (Cyc), M1 macrophages (M1Mφ), M1 monocytes (M1Mo), dendritic-like cells (DC), macrophages showed strong upregulation of interferon (IFN)-induced genes (MAC-IFNIC), M2 macrophages (M2Mφ), cardiac tissue-resident Mφ (MAC-TR), T-cells (TC), B-cells (BC), natural killer cells (NKC), glial cells (Glial). As noted above, granulocytes were not included in the datasets. The values of GRN expression in individual cell types were extracted and statistically analyzed.

2.17 | Statistical analysis

Data were shown as mean ± SEM. Quantitative variables were statistically analyzed using Levene's test followed by Student's or Welch's two-tailed *t*-test for two-group comparisons, and one-way ANOVA followed by Tukey's or Dunnett's post hoc test for multiple pair-wise comparisons. The *p*-value of <0.05 was considered statistically significant. All statistical analyses were performed using SPSS (version 24.0.0.0; IBM, Armonk, NY, USA) software and GraphPad Prism (version 9.5.1; GraphPad Software, Boston, MA, USA).

3 | RESULTS

3.1 | Progranulin is abundantly expressed in macrophages following MI

First, we investigated Progranulin (PGRN) expression levels in the whole heart after MI. PGRN expression significantly increased at 1, 3, and 7 days after MI (Figure 1A,B). We also evaluated PGRN localization post-MI

by immunostaining of transverse myocardial sections. The areas were classified as infarct, border, and remote (Figure 1C). The fluorescence intensity of PGRN significantly increased at the border and infarct areas 3 days after MI (Figure 1D,E). Temporal alterations in PGRN expression correspond to macrophage accumulation following MI.[7] Then, we performed immunostaining for PGRN and CD68 to examine the cells expressing PGRN. PGRN co-localized with CD68, which is a marker of macrophages (Figure 1F). $CD68^{+}$ cells and $PGRN^{+}$

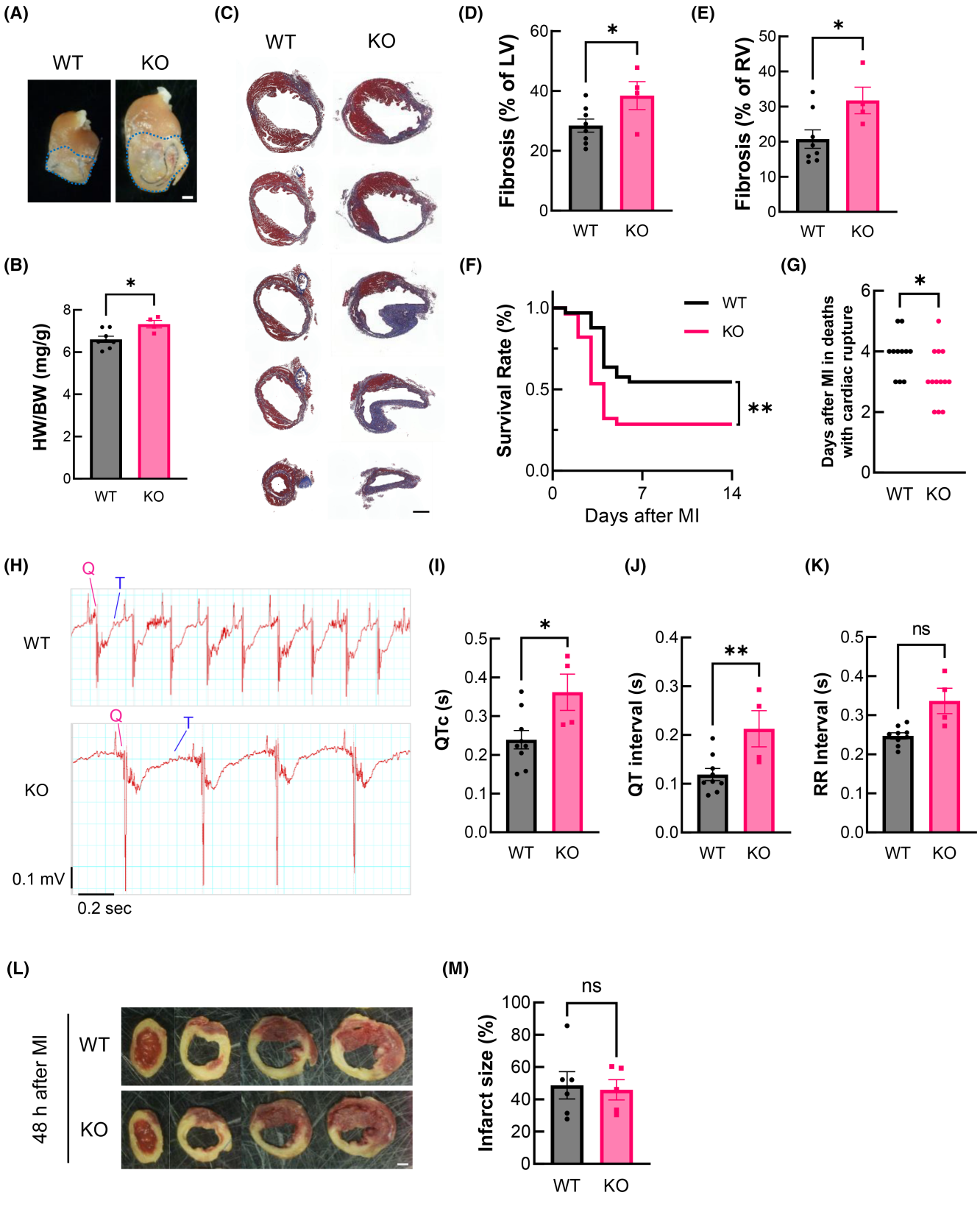

FIGURE 2 Adverse histological and electrophysiological cardiac remodeling after MI in PGRN-KO mice. (A) Typical images of the whole hearts in WT and PGRN-KO mice at 14 days post-MI. Scale Bars: 1 mm. (B) Quantitative analysis of heart weight per body weight (HW/BW). (C) Typical images of the myocardial transverse sections from apex to ligature visualized by Masson's trichrome staining in WT and PGRN-KO mice at 14 days after MI. Scale Bars: 1 mm. (D, E) Quantitative analysis of fibrosis size (%) in left and right ventricular (LV and RV). Data are the means ± SEM (WT: $n = 8$, KO: $n = 4$). *$p < 0.05$ versus WT (Levene's test followed by Student's two-tailed t-test). (F) Kaplan–Meier survival curves in WT and PGRN-KO mice following MI. Data are the means ± SEM (WT: $n = 33$, PGRN-KO: $n = 28$). **$p < 0.01$ versus WT (Log-rank test). (G) Observed days of cardiac rupture post-MI. Data are the means ± SEM (WT: $n = 11$, PGRN-KO: $n = 13$). *$p < 0.05$ versus WT (Mann–Whitney U test). (H) Electrocardiograms (ECGs) in WT and PGRN-KO mice at 14 days after MI. (I–K) Quantitative analysis of corrected QT interval (QTc), QT interval, and RR interval, respectively. Data are the means ± SEM (WT: $n = 9$, PGRN-KO: $n = 4$). *$p < 0.05$, **$p < 0.01$ versus WT (Levene's test followed by Student's or Welch's two-tailed t-test). (L, M) Typical images of infarct myocardium and quantification of left ventricular (LV) infarct size in WT and PGRN-KO mice at 48 h after MI. Data are the means ± SEM (WT: $n = 5$, PGRN-KO: $n = 6$). N.S versus WT (Levene's test followed by Student's two-tailed t-test).

$CD68^+$ cells significantly increased at the border areas at 3 days post-MI (Figure 1G–I). The ratio of $PGRN^+$ cells to $CD68^+$ cells was approximately 79.6% and 68.5% after MI and sham operation, respectively (Figure 1J). We also analyzed the clusters and cells expressing PGRN using publicly available datasets of single-cell RNA-seq (scRNA-seq).[30] PGRN expression levels were significantly higher in the cluster of Monocyte and Macrophage not only at 3 days post-MI, but also at 7 days post-MI and in the sham-operated group (Figure 1K, and Supporting Information Figure S1A,B). These findings suggest that increased expression of PGRN predominantly depends on macrophages following MI.

3.2 | Progranulin deficiency induces high mortality, cardiac fibrosis, and severe arrhythmias after MI

We investigated the role of PGRN on post-MI pathophysiology using PGRN-KO mice. Post-MI severity is associated with increased cardiac hypertrophy, which is shown as the heart weight per body weight ratio (HW/BW).[31,32] HW/BW significantly increased in PGRN-KO mice compared to WT mice at 2 weeks after MI (Figure 2A,B). Excessive fibrotic response contributes to contractile dysfunction and severe arrhythmias due to increased ventricular stiffness and impaired mechanoelectrical coupling of cardiomyocytes.[6,33] We also evaluated the fibrosis size in the left and right ventricles (LV and RV) by Masson's trichrome staining, which dyes collagen-rich fibrotic regions blue (Figure 2C). LV and RV fibrosis size significantly increased in PGRN-KO mice compared to WT mice after MI (Figure 2D,E). PGRN-KO mice also showed severely lower survival rates post-MI, and earlier deaths due to cardiac rupture (Figure 2F,G). In addition, we analyzed electrocardiogram (ECG) as an index of cardiac function (Figure 2H). Corrected QT interval (QTc) and QT interval were prolonged in PGRN-KO mice 14 days after MI (Figure 2I,J). There was a tendency for an increase but no significant difference of RR interval in PGRN-KO mice compared to WT mice (Figure 2K). Prolonged QT interval, which reflects the duration required for the recovery of ventricular electrical excitation, reduces the efficiency of the cardiac contraction and relaxation, potentially inducing lethal arrhythmias.[34] PGRN deficiency has the potential to induce more severe arrhythmia and indirectly cardiac dysfunction following MI. Taken together, PGRN deficiency could lead to histological abnormalities and electrophysiological dysfunction following MI. Then, we evaluated infarct size shown as an index of cardiomyocyte deaths at the acute phase following MI. There was no significant difference in infarct size between WT and PGRN-KO mice at 48 h after MI (Figure 2L,M). We also examine the effects of PGRN on cardiomyocyte hypertrophy in H9c2 treated with Angiotensin II (Ang II) for 24 h. PGRN treatment significantly reduced an increase of cardiomyocyte surface areas stimulated by Ang II (Supporting Information Figure S2A,B). These findings suggest that adverse cardiac remodeling by loss of PGRN is attributed to not increased cardiomyocyte deaths at the acute phase but subsequent pathological processes following MI.

3.3 | Macrophage-related alteration in PGRN-KO mice following MI

PGRN-KO mice showed higher mortality from 3 days post-MI. Considering that it is important to understand the pathophysiology involved, we focused on the day 3 post-MI. In a previous report, PGRN deficiency induced M2-like macrophages in the injured muscle.[21] Then, we investigated whether loss of PGRN affects macrophage properties post-MI. CD206 is known as a marker of M2-like macrophages.[8,35] PGRN-deficient myocardium exhibited higher levels of CD206, MerTK expression at 3 days following MI (Figure 3A,B). There were no significant differences in the expression levels of CD206 and

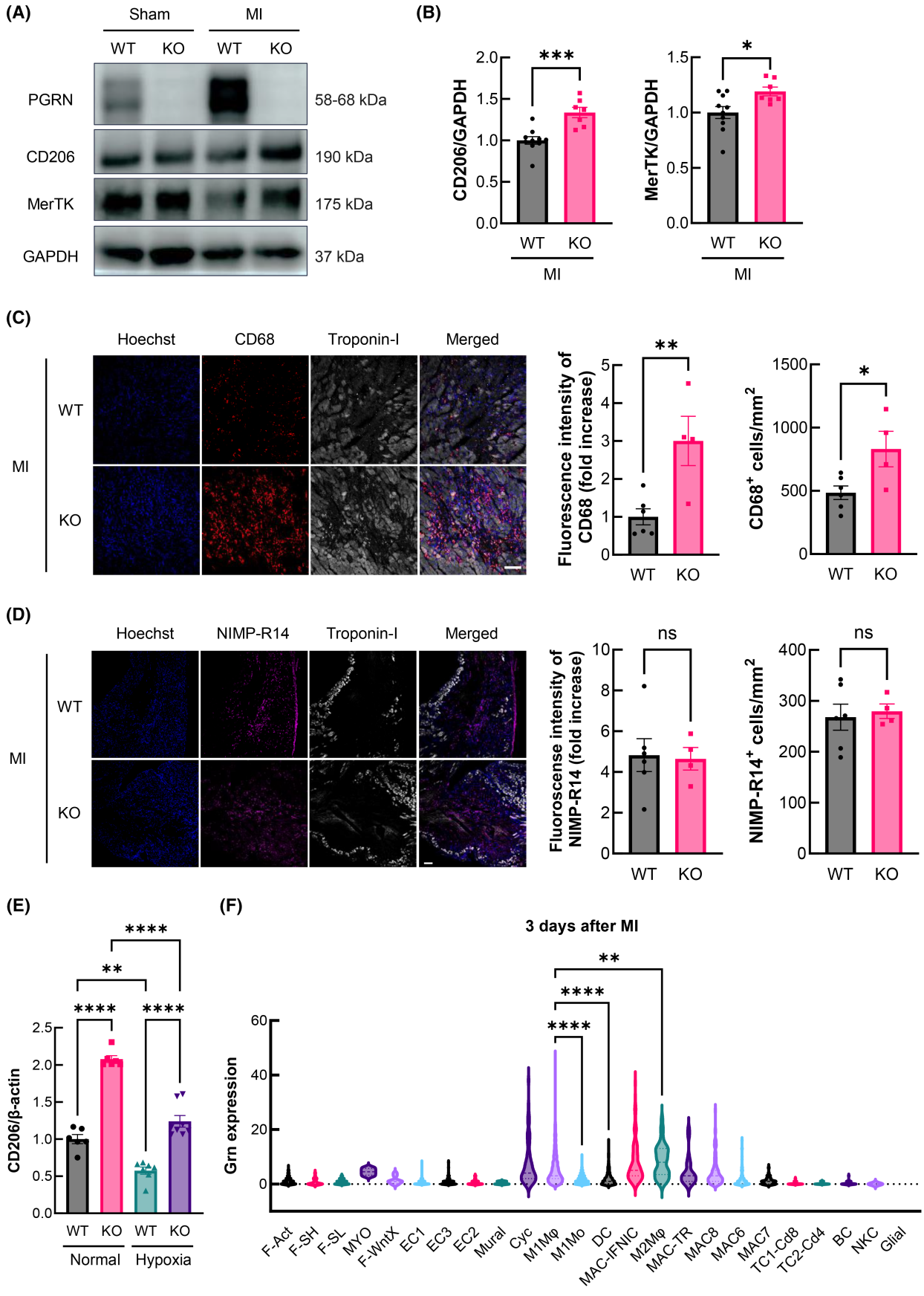
(A)
Sham
MI
WT
KO
WT
KO
PGRN
CD206
MerTK
GAPDH
58-68 kDa
190 kDa
175 kDa
37 kDa
(B)
CD206/GAPDH
MerTK/GAPDH
***
*
WT
KO
MI
(C)
Hoechst
CD68
Troponin-I
Merged
MI
WT
KO
Fluorescence intensity of CD68 (fold increase)
CD68+ cells/mm2
**
*
(D)
Hoechst
NIMP-R14
Troponin-I
Merged
Fluoroscense intensity of NIMP-R14 (fold increase)
NIMP-R14+ cells/mm2
ns
(E)
CD206/β-actin
****
**
Normal
Hypoxia
(F)
3 days after MI
Grn expression
F-Act
F-SH
F-SL
MYO
F-WntX
EC1
EC3
EC2
Mural
Cyc
M1Mφ
M1Mo
DC
MAC-IFNIC
M2Mφ
MAC-TR
MAC8
MAC6
MAC7
TC1-Cd8
TC2-Cd4
BC
NKC
Glial

FIGURE 3 Alteration of protein expression and macrophage accumulation affected by PGRN deficiency following MI. (A) Immunoblots exhibit PGRN (58–68 kDa), CD206 (190 kDa), and MerTK (175 kDa) in whole hearts of WT and PGRN-KO mice at 3 days after MI. (B) Quantitative analysis of CD206 and MerTK expression levels normalized to GAPDH, in the entire myocardium at 3 days post-MI. Data are the means ± SEM (WT: $n = 10$, PGRN-KO: $n = 7$). $^{*}p < 0.05$, $^{***}p < 0.001$ versus WT (Levene's test followed by Student's or Welch's two-tailed *t*-test). (C) Typical confocal microscopic images (×20 magnification) of macrophages at border areas in WT and PGRN-KO mice at 3 days after MI. Blue: nuclei stained with Hoechst 33342, Red: CD68, Gray: Troponin-I. Scale bar: 100 μm. Quantitative analysis of fluorescence intensity of CD68 and the number of CD86+ cells at border areas in WT and PGRN-KO mice at 3 days post-MI. Data are the means ± SEM (WT: $n = 6$, PGRN-KO: $n = 4$). $^{*}p < 0.05$, $^{**}p < 0.01$ versus WT (Levene's test followed by Student's or Welch's two-tailed *t*-test). (D) Representative confocal microscopic images (×10 magnification) of neutrophils at border areas in WT and PGRN-KO mice at 3 days after MI. Cyan: nuclei stained with Hoechst 33342, Magenta: NIMP-R14, Green: Troponin-I. Scale bar: 100 μm. Data are the means ± SEM (WT: $n = 6$, PGRN-KO: $n = 4$). N.S versus WT (Levene's test followed by Student's two-tailed *t*-test). (E) mRNA levels of CD206 in peritoneal macrophages in WT and PGRN-KO under normal and hypoxic conditions. Data are the means ± SEM (Normal; WT: $n = 6$, KO: $n = 6$, Hypoxia; WT: $n = 7$, PGRN-KO: $n = 8$). $^{**}p < 0.01$, $^{***}p < 0.001$, $^{***}p < 0.0001$ versus WT (one-way ANOVA followed by Dunnett T3 test). (F) scRNA-seq analysis of cells expressing Granulin (GRN) gene at 3 days post-MI. Data are the means ± SEM (n = F-Act: 185, F-SH: 25, F-SL: 40, MYO: 4, F-WntX: 8, EC1: 162, EC2: 37, EC3: 75, Mural: 10, Cyc: 71, M1Mφ: 1964, M1Mo: 493, DC: 271, MAC-IFNIC: 125, M2Mφ: 49, MAC-TR: 23, MAC6: 110, MAC7: 43, MAC8: 106, TC1-Cd8: 28, TC2-Cd4: 16, BC: 27, NKC: 2, Glial: 1). $^{**}p < 0.01$, $^{****}p < 0.0001$ versus M1Mφ (one-way ANOVA followed by Tuckey's test).

MerTK between WT and PGRN-KO mice in the sham-operated groups (Supporting Information Figure S3A). We evaluated the accumulation of macrophages and neutrophils at border areas at 3 days post-MI. PGRN deficiency significantly increased the fluorescence intensity of CD68 and the number of $CD68^{+}$ cells (Figure 3C). There was no significant difference in the fluorescence intensity of NIMP-R14 and the number of NIMP-$R14^{+}$ cells (Figure 3D). To examine the macrophage polarization, peritoneal macrophages were obtained from WT and PGRN-KO mice. The levels of CD206 expression were significantly higher in PGRN-KO macrophages compared to WT macrophages under normal and hypoxic conditions (Figure 3E). To understand the relationship between PGRN and macrophage phenotypes, we also analyzed the cells expressing PGRN after MI using publicly available datasets of scRNA-seq.[30] M2 macrophages exhibited higher expression of PGRN than other cells including M1 monocyte (M1Mo) and dendritic cell (DC), and M1 macrophages at 3 days after MI (Figure 3F). A similar tendency was shown at 7 days after MI and in sham operation (Supporting Information Figure S4A,B). The levels of COX2 and MMP-9 were lower and p-Akt was higher in PGRN-deficient myocardium at 3 days post-MI (Supporting Information Figure S5A,B). These expression levels were not significantly changed in sham-operated groups (Supporting Information Figure S5C). We also examine CCL2 and αSMA expression levels to understand the mechanism of macrophage infiltration and fibrotic remodeling (Supporting Information Figure S5D). Their expression levels were not altered by PGRN deficiency at 3 days following MI and sham operation (Supporting Information Figure S5E,F). Overall, PGRN could regulate M2-like macrophage polarization after MI.

3.4 | Abnormal subpopulation of macrophages in PGRN-deficient myocardium

It is important to understand whether the higher levels of CD206 and MerTK expression depend on increased expression in individual cells or the number of cells in PGRN-deficient myocardium. Then, we performed a flow cytometric analysis to reveal the relationship between macrophage subpopulations and expression levels of CD206 and MerTK. First, PGRN-KO mice had a higher proportion of $CD11b^{+}$ cells in singlet cells. Cardiac $CCR2^{+}$ macrophages are differentiated from bone marrow-derived circulating monocytes, which shift from initial $Ly6C^{high}$ inflammatory macrophages to $Ly6C^{low}$ reparative macrophages in injured tissue.[36] PGRN deficiency induced especially markedly higher proportion of $Ly6C^{-}$ $CCR2^{+}$ $CD11b^{+}$ in singlet cells at 3 days after MI (Figure 4C,D and Supporting Information Figure S6). Importantly, CD206 and MerTK were almost simultaneously expressed in this subpopulation (Figure 4E,F and Supporting Information Figure S6). In other words, the proportion of $CD206^{+}$ $Ly6C^{-}$ $CCR2^{+}$ $CD11b^{+}$ and $MerTK^{+}$ $Ly6C^{-}$ $CCR2^{+}$ $CD11b^{+}$ in singlet cells were also significantly higher in PGRN-deficient myocardium following MI (Figure 4G,H). On the other hand, there were no significant differences of the proportion in each of the three subpopulations; defined as $Ly6C^{+}$ $CCR2^{+}$ $CD11b^{+}$, $Ly6C^{+}$ $CCR2^{-}$ $CD11b^{+}$, and $Ly6C^{-}$ $CCR2^{-}$ $CD11b^{+}$, in singlet cells between both groups (Supporting Information Figure S7A). There were also no significant differences in CD206 and MerTK expression levels in individual cells that are defined as $Ly6C^{-}$ $CCR2^{+}$ $CD11b^{+}$ between both groups (Supporting Information Figure S7B). Differentiated

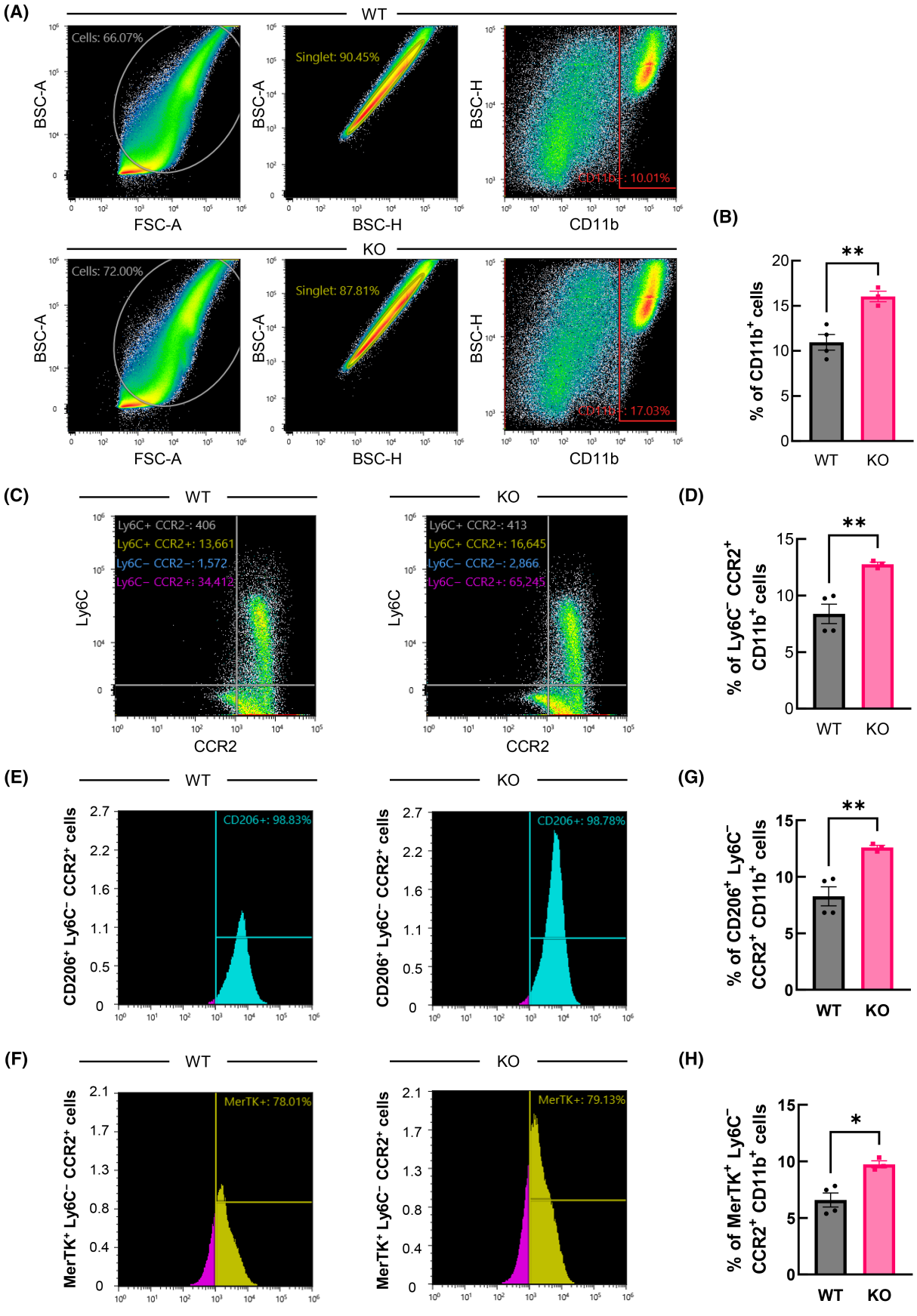
(A)
WT
Cells: 66.07%
Singlet: 90.45%
CD11b+: 10.01%
KO
Cells: 72.00%
Singlet: 87.81%
CD11b+: 17.03%
FSC-A
BSC-A
BSC-H
CD11b
(B)
% of CD11b+ cells
WT
KO
(C)
Ly6C+ CCR2-: 406
Ly6C+ CCR2+: 13,661
Ly6C− CCR2−: 1,572
Ly6C− CCR2+: 34,412
Ly6C+ CCR2-: 413
Ly6C+ CCR2+: 16,645
Ly6C− CCR2−: 2,866
Ly6C− CCR2+: 65,245
Ly6C
CCR2
(D)
% of Ly6C− CCR2+ CD11b+ cells
(E)
CD206+: 98.83%
CD206+: 98.78%
CD206+ Ly6C− CCR2+ cells
(G)
% of CD206+ Ly6C− CCR2+ CD11b+ cells
(F)
MerTK+: 78.01%
MerTK+: 79.13%
MerTK+ Ly6C− CCR2+ cells
(H)
% of MerTK+ Ly6C− CCR2+ CD11b+ cells

FIGURE 4 Abnormal subpopulation of cardiac macrophages in PGRN-KO mice post-MI. (A, B) Representative FACS plots of CD11b+ cells and quantified ratio of CD11b+ cells in total singlet cells in WT and PGRN-KO mice 3 days following MI. (C) Representative FACS plots of cells distinguished by expression levels of Ly6C and CCR2. (D) Quantified proportion of Ly6C$^-$ CCR2+ CD11b+ cells in singlet cells. (E, F) Representative histograms of CD206+ and MerTK+ cells in Ly6C$^-$ CCR2+ macrophages. (G, H) Quantified proportion of CD206+ Ly6C$^-$ CCR2+ CD11b+ and MerTK+ Ly6C$^-$ CCR2+ CD11b+ cells in singlet cells. Data are the means ± SEM (WT: $n = 4$, PGRN-KO: $n = 3$). $^*p < 0.05$, $^{**}p < 0.01$ versus WT (Levene's test followed by Student's two-tailed t-test).

macrophages, rather than inflammatory monocytes may markedly accumulate in PGRN-deficient myocardium at 3 days after MI. These findings suggest that the higher levels of CD206 and MerTK expression in PGRN-deficient myocardium depend on the increased number of M2-like macrophages, rather than expression levels in individual macrophages.

3.5 | PGRN deficiency induces abnormal polarization in inflammatory response

Following the inflammatory response, macrophages are self-resolved and induced to M2-like phenotypes. We also investigated the effects of PGRN deficiency on macrophage polarization using bone marrow-derived macrophages (BMDMs). M1 and M2 macrophages were induced by treatment with LPS + IFN-γ and IL-4 for 48 h, respectively, and then RT-qPCR was performed. First, the levels of PGRN expression significantly increased in BMDMs treated with LPS + IFN-γ (Figure 5A). Then, we evaluated the expression levels of inflammatory cytokines in WT and PGRN-deficient BMDMs at 48 h following stimulation of LPS + IFN-γ and IL-4 (Figure 5B–E). PGRN-deficient BMDMs showed lower levels of IL-1β after LPS + IFN-γ treatment (Figure 5B). There were no significant differences of IL-6, TNF-α, and CCL2 expression levels between WT and PGRN-deficient BMDMs treated with LPS + IFN-γ (Figure 5C–E). Meanwhile, we also examine the expression levels of M2-like macrophage markers (Figure 5F–I). PGRN-deficient BMDMs exhibited lower levels of IL-10, and higher levels of TGF-β and IL-4R than WT BMDM at 48 h following stimulation of LPS + IFN-γ (Figure 5F, H). The expression levels of IL-6, TNF-α, CCL2, and CD206 were not changed in both BMDMs treated with LPS + IFN-γ (Figure 5C,D,E,I). There were no significant differences in all the expression levels between both BMDMs following IL-4 stimulation. LPS-induced phagocytosis was also evaluated in WT and PGRN-deficient BMDMs. Phagocytosis increased in PGRN-deficient BMDMs compared to WT BMDMs at 1 h after LPS treatment (Figure 5J). There were no significant changes at 6 and 24 h between both BMDMs treated with LPS (Figure 5K,L). Collectively, PGRN-deficient BMDMs could exhibit further phagocytosis at the acute phase but have profibrotic rather than proinflammatory phenotypes at the late phase following inflammation.

4 | DISCUSSION

In the present study, we aimed to determine the impact of PGRN genetic deletion on cardiac remodeling post-MI. PGRN was abundantly expressed in infiltrating macrophages at the border areas following MI. PGRN deficiency contributed to higher mortality, increased fibrosis, and severe arrhythmias post-MI. PGRN-deficient myocardium showed higher levels of CD206 and MerTK expression, which is associated with an increased subpopulation of Ly6C$^-$ CCR2$^+$ CD11b$^+$ macrophages. On the other hand, PGRN expression was induced in BMDMs by LPS + IFN-γ treatment. PGRN deficiency increased IL-4R and TGF-β expression levels, reduced IL-1β and IL-10 expression levels, and stimulated earlier activation of phagocytosis in BMDMs treated with LPS and IFN-γ. Here, we revealed that PGRN plays a cardioprotective role in adverse cardiac remodeling after MI, which is partially mediated by regulating inflammatory response in macrophages.

Fibrosis of not only LV but also RV further increased in PGRN-KO mice post-MI. Cardiac fibrosis in remote areas after MI is reactive fibrosis, which is caused by myofibroblast activation.[37] In a previous report, PGRN treatment has suppressed TGF-β-induced gene expression of αSMA and Col1a1 in human primary stellate cells that are hepatic fibroblasts.[38] Excessive fibrosis by loss of PGRN may attributed to inadequate suppression of fibroblast activation post-MI. PGRN deficiency did not alter αSMA expression at 3 days after MI. Fibroblasts are activated in the myocardium at 3 days post-MI and differentiated into myofibroblasts, which actively secrete extracellular matrix proteins.[39] Considering these findings, PGRN could inhibit fibroblast activation, but not significantly affect early activation of fibroblasts following MI. PGRN treatment reduced Angiotensin II (Ang II)-induced cardiomyocyte hypertrophy. PGRN knockdown has previously increased hypertrophy in primary neonatal rat ventricular myocytes.[40] PGRN may inhibit cardiomyocyte hypertrophy. Taken together, post-MI cardiac tissue hypertrophy by PGRN deficiency

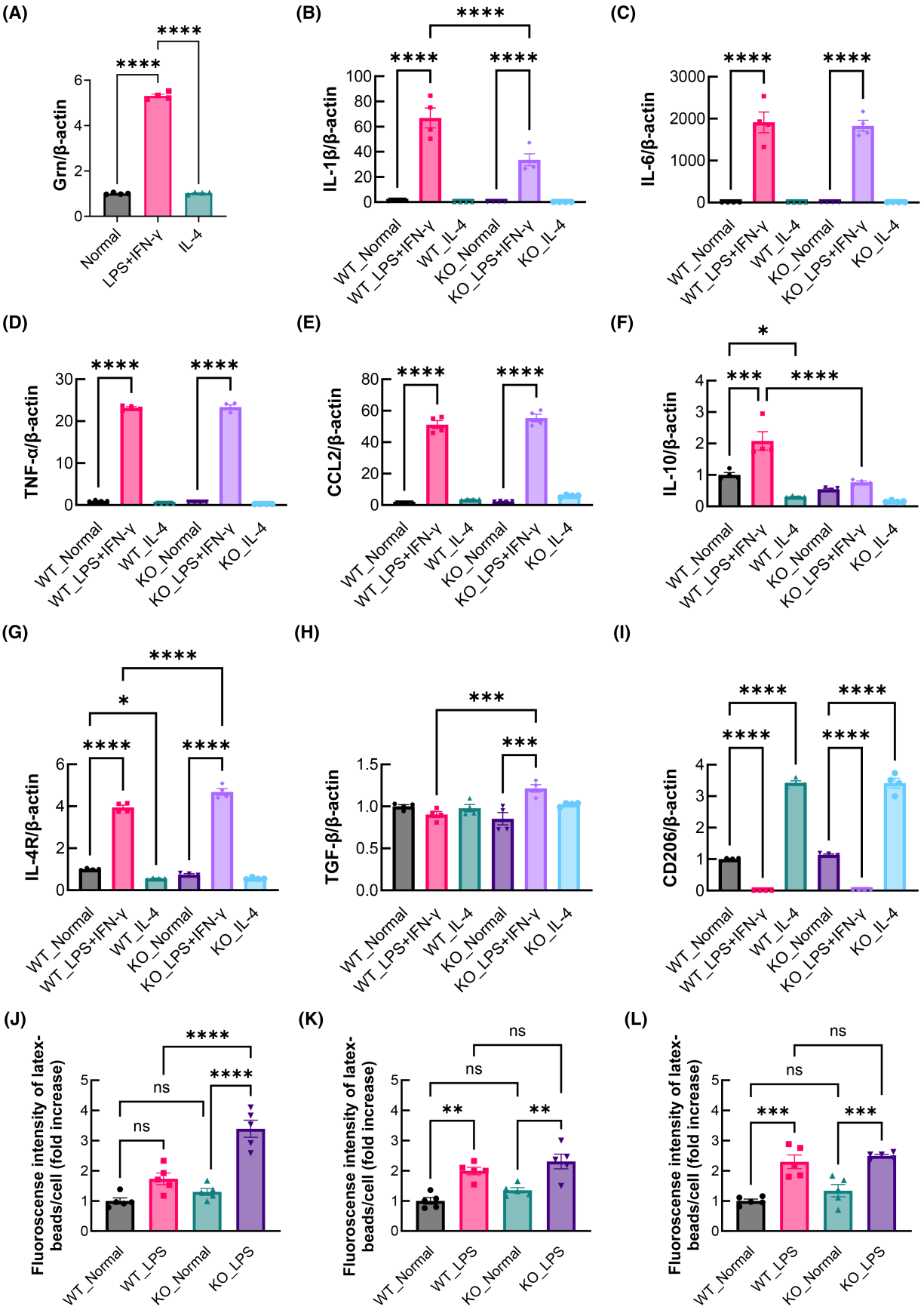
(A)
Grn/β-actin
Normal
LPS+IFN-γ
IL-4
(B)
IL-1β/β-actin
(C)
IL-6/β-actin
(D)
TNF-α/β-actin
(E)
CCL2/β-actin
(F)
IL-10/β-actin
(G)
IL-4R/β-actin
(H)
TGF-β/β-actin
(I)
CD206/β-actin
WT_Normal
WT_LPS+IFN-γ
WT_IL-4
KO_Normal
KO_LPS+IFN-γ
KO_IL-4
(J)
(K)
(L)
Fluoroscense intensity of latex-beads/cell (fold increase)
WT_Normal
WT_LPS
KO_Normal
KO_LPS
ns

FIGURE 5 Abnormal polarization of PGRN-deficient bone marrow-derived macrophages in inflammatory responses. (A) Granulin (GRN) mRNA levels in bone marrow-derived macrophages (BMDMs), treated with LPS + IFN-γ and IL-4 for 48 h. Data are the means ± SEM (Normal: $n = 4$, LPS + IFN-γ: $n = 4$, IL-4: $n = 4$). ****$p < 0.0001$ versus LPS+ IFN-γ (one-way ANOVA followed by Dunnett T3 test). (B–I) mRNA levels of IL-1β, IL-6, TNF-α, CCL2, IL-10, IL-4R, TGF-β, and CD206 in WT and PGRN-deficient BMDMs treated with LPS + IFN-γ and IL-4 for 48 h, respectively. Data are the means ± SEM (WT; Normal: $n = 4$, LPS + IFN-γ: $n = 4$, IL-4: $n = 4$, PGRN-KO; Normal: $n = 4$, LPS + IFN-γ: $n = 4$, IL-4: $n = 4$). **$p < 0.05$, **$p < 0.01$, ***$p < 0.001$, ****$p < 0.0001$ (one-way ANOVA followed by Tuckey's test). (J–L) Phagocytosis activities quantified by fluorescence intensity of latex-microbeads corrected by the number of cells in WT and PGRN-deficient BMDMs treated with LPS for 1, 6, and 24 h. Data are the means ± SEM (WT; Normal: $n = 5$, LPS: $n = 5$, PGRN-KO; Normal: $n = 5$, LPS: $n = 5$). **$p < 0.01$, ***$p < 0.001$, ****$p < 0.0001$ (one-way ANOVA followed by Tuckey's test).

may arise from fibrotic scar thickening and cardiomyocyte hypertrophy.

Following myocardial necrosis caused by the occlusion of coronary arteries, the inflammatory response is immediately initiated to recruit monocytes/macrophages to the infarcted myocardium.[41] Monocytes/Macrophages are attracted to chemokines such as C–C motif chemokine ligand 2 (CCL2).[42,43] PGRN was abundantly expressed in macrophages rather than other cells in scRNA-seq analysis. Macrophage infiltration further increased in PGRN-deficient myocardium following MI, which was attributed to CCR^+ bone marrow-derived macrophages. However, CCL2 expression had a tendency for an increase but was not significantly changed by PGRN deficiency. Expression levels of CCL2 mRNA have previously increased at early phase, 4- and 10-hours post-MI.[44] CCL2 may be largely involved earlier than day 3 post-MI. Because increased macrophage infiltration may be attributed to the overall effects of cytokines and chemokines altered by PGRN deficiency, future studies are required for this concern through comprehensive analysis.

MerTK is a phagocytosis receptor expressed mainly in macrophages, which recognizes the debris of apoptotic cells.[9] Inadequate removal of apoptotic cells by MerTK-deficient macrophages has resulted in prolonged inflammation after MI, increased cardiac fibrosis, and reduced cardiac function. PGRN deficiency induced higher levels of MerTK expression but increased mortality following MI. Further increased phagocytosis was also observed in PGRN-deficient BMDMs at 1 h rather than at 6 and 24 h after inflammatory response. In previous reports, loss of PGRN enhanced phagocytosis in BMDMs and microglia.[14,45] These findings indicate that PGRN regulates phagocytosis activity at the earlier inflammatory phase. PGRN-KO mice also had earlier cardiac rupture following MI. Post-MI cardiac rupture has decreased by MMP-2 deficiency, which delays phagocytic removal of apoptotic cardiomyocytes by macrophages.[46] Considering these results, earlier activation of macrophage phagocytosis by loss of PGRN may cause an imbalance of clearance of apoptotic cells and scar formation, leading to vulnerability of the myocardium.

Higher levels of CD206 expression were observed in PGRN-deficient myocardium and peritoneal macrophages. PGRN-KO mice have exhibited M2-like macrophages expressing CD206 after cardiotoxin-induced skeletal muscle injury.[21] Loss of PGRN may enhance M2-like polarization in response to tissue injury and niche. Macrophages exhibit self-control over their polarization from M1- to M2-like phenotype following inflammatory response.[47] Actually, peritoneal macrophages in the resolution phase after inflammation have expressed simultaneously M2 markers and M1 markers.[48] PGRN deficiency has previously triggered M1-like macrophages, which actively secrete proinflammatory cytokines after LPS stimulation.[20] In the present study, PGRN-deficient BMDMs showed higher levels of IL-4R expression after inflammation. IL-4R plays a key role in the transition to M2 macrophages.[49] Suppressive feedback for inflammation may be initiated earlier in macrophages by the absence of PGRN. On the other hand, IL-10 is known as an anti-inflammatory cytokine, which enhances M2-like polarization in macrophages.[8] In PGRN-deficient BMDMs, IL-10 levels were lower following inflammation and a tendency for a decline at baseline. PGRN has been reported to ameliorate colitis through IL-10 signaling.[50] IL-10 has inhibited TLR4-induced activation in macrophages.[51] Considering these findings, abnormal susceptibility to inflammation and subsequent resolution may be partially due to dysfunction of IL-10 in PGRN-deficient macrophages. These findings suggest that loss of PGRN impairs the resolution responses after inflammation in macrophages.

$CD206^+$ M2-like macrophages promote cardiac repair and generally contribute to improved prognosis.[49] However, PGRN-KO mice exhibited higher mortality, increased fibrosis, and severe arrhythmias, regardless of increased CD206 expression following MI. The macrophages expressing CD206 were included in $CCR2^+$ $Ly6C^-$ macrophage subpopulation that is classified as bone marrow-derived anti-inflammatory properties. Bone marrow-derived $Ly6C^-$ macrophages have previously stimulated fibrosis and contributed to the worsening of pathological conditions in the kidney after ischemic injury.[52] Increased cardiac $CCR2^+$ $Ly6C^-$ macrophages may exacerbate cardiac

fibrosis and reduce survival in PGRN-KO mice after MI. Reduced infiltrating macrophages by CCL2 deficiency have decreased cardiac fibrosis at 7 days following ischemia/reperfusion injury.[53] Macrophage has a key role in fibrotic scar formation at early phase post-MI. TGF-β expression levels also increased in PGRN-deficient BMDMs after inflammation. Considering these findings, PGRN may suppress excessive cardiac fibrosis by regulating profibrotic response in macrophages following inflammation caused by ischemic injury.

In conclusion, we suggest that PGRN prevents the progression of HF after MI by modulating macrophage function. PGRN could play an important role in appropriate cardiac remodeling after MI.

AUTHOR CONTRIBUTIONS

Takahiro Sasaki and Hideaki Hara conceived and designed the research. Takahiro Sasaki performed the research and acquired the data. Takahiro Sasaki, Yoshiki Kuse, Shinsuke Nakamura, and Masamitsu Shimazawa analyzed and interpreted the data. All authors were involved in drafting and revising the manuscript.

ACKNOWLEDGMENTS

This work was supported by JSPS KAKENHI Grant Number JP21J23271.

DISCLOSURES

The authors declare no conflicts of interest.

DATA AVAILABILITY STATEMENT

Data sharing is not applicable to this article as no datasets were generated or analyzed during the current study.

REFERENCES

1. Roth GA, Mensah GA, Johnson CO, et al. Global burden of cardiovascular diseases and risk factors, 1990-2019: update from the GBD 2019 study. *J Am Coll Cardiol*. 2020;76:2982-3021.
2. World Health Organization. Cardiovascular diseases (CVDs). Retrieved from 2021, June 11 https://www.who.int/news-room/fact-sheets/detail/cardiovascular-diseases-(cvds)
3. Thygesen K, Alpert JS, Jaffe AS, et al. Fourth universal definition of myocardial infarction (2018). *Circulation*. 2018;138:237-269.
4. Spencer FA, Meyer TE, Gore JM, Goldberg RJ. Heterogeneity in the management and outcomes of patients with acute myocardial infarction complicated by heart failure: the national registry of myocardial infarction. *Circulation*. 2002;105:2605-2610.
5. Prabhu SD, Frangogiannis NG. The biological basis for cardiac repair after myocardial infarction. *Circ Res*. 2016;119:91-112.
6. Weil BR, Neelamegham S. Selectins and immune cells in aucte mycardial infarction and post-infarction ventricular remodelings: pathophysiology and novel treatments. *Front Immunol*. 2019;10:1-15.
7. Yan X, Anzai A, Katsumata Y, et al. Temporal dynamics of cardiac immune cell accumulation following acute myocardial infarction. *J Mol Cell Cardiol*. 2013;62:24-35.
8. Kim Y, Nurakhayev S, Nurkesh A, Zharkinbekov Z, Saparov A. Macrophage polarization in cardiac tissue repair following myocardial infarction. *Int J Mol Sci*. 2021;22:1-15.
9. Wan E, Yeap XY, Dehn S, et al. Enhanced efferocytosis of apoptotic cardiomyocytes through myeloid-epithelial-reproductive tyrosine kinase links acute inflammation resolution to cardiac repair after infarction. *Circ Res*. 2013;113:1004-1012.
10. Kessenbrock K, Plaks V, Werb Z. Matrix metalloproteinases: regulators of the tumor microenvironment. *Cell*. 2010;141:52-67.
11. Shivshankar P, Halade GV, Calhoun C, et al. Caveolin-1 deletion exacerbates cardiac interstitial fibrosis by promoting M2 macrophage activation in mice after myocardial infarction. *Curr Ther Res – Clin Exp*. 2014;76:84-93.
12. Bateman A, Bennett HPJ. Granulins: the structure and function of an emerging family of growth factors. *J Endocrinol*. 1998;158:145-151.
13. He Z, Ong CHP, Halper J, Bateman A. Progranulin is a mediator of the wound response. *Nat Med*. 2003;9:225-229.
14. Schmitz K, Wilken-Schmitz A, Vasic V, Brunkhorst R, Schmidt M, Tegeder I. Progranulin deficiency confers resistance to autoimmune encephalomyelitis in mice. *Cell Mol Immunol*. 2020;17:1077-1091.
15. Chantry D, DeMaggio AJ, Brammer H, et al. Profile of human macrophage transcripts: insights into macrophage biology and identification of novel chemokines. *J Leukoc Biol*. 1998;64:49-54.
16. Subrahmanyam YVBK, Yamaga S, Prashar Y, et al. RNA expression patterns change dramatically in human neutrophils exposed to bacteria. *Blood*. 2001;97:2457-2468.
17. Egashira Y, Suzuki Y, Azuma Y, et al. The growth factor progranulin attenuates neuronal injury induced by cerebral ischemia-reperfusion through the suppression of neutrophil recruitment. *J Neuroinflammation*. 2013;10:2-13.
18. Zhou M, Tang W, Fu Y, et al. Progranulin protects against renal ischemia/reperfusion injury in mice. *Kidney Int*. 2015;87:918-929.
19. Sasaki T, Shimazawa M, Kanamori H, et al. Effects of progranulin on the pathological conditions in experimental myocardial infarction model. *Sci Rep*. 2020;10:1-13.
20. Yu Y, Xu X, Liu L, et al. Progranulin deficiency leads to severe inflammation, lung injury and cell death in a mouse model of endotoxic shock. *J Cell Mol Med*. 2016;20:506-517.
21. Sugihara H, Miyaji K, Yamanouchi K, Matsuwaki T, Nishihara M. Progranulin deficiency leads to prolonged persistence of macrophages, accompanied with myofiber hypertrophy in regenerating muscle. *J Vet Med Sci*. 2018;80:346-353.
22. Kayasuga Y, Chiba S, Suzuki M, et al. Alteration of behavioural phenotype in mice by targeted disruption of the progranulin gene. *Behav Brain Res*. 2007;185:110-118.
23. Lindsey ML, Bolli R, Canty JM, et al. Guidelines for experimental models of myocardial ischemia and infarction. *Am J Physiol – Hear Circ Physiol*. 2018;314:H812-H838.
24. Das S, Goldstone AB, Wanget H, et al. A unique collateral artery development program promotes neonatal heart regeneration. *Cell*. 2019;176:1128-1142.e18.
25. Merentie M, Lottonen-Raikaslehto L, Ylä-Herttuala S. Development and validation of ECG analysis algorithm in

mice. *Conn's Handbook of Models for Human Aging*. Elsevier Inc.; 2018:271-285.
26. Speerschneider T, Thomsen MB. Physiology and analysis of the electrocardiographic T wave in mice. *Acta Physiol*. 2013;209:262-271.
27. Aronoff L, Epelman S, Clemente-Casares X. Isolation and identification of extravascular immune cells of the heart. *J Vis Exp*. 2018;2018:1-7.
28. Li S, Li L, Chen J, et al. Liposomal honokiol inhibits glioblastoma growth through regulating macrophage polarization. *Ann Transl Med*. 2021;9:1644.
29. Cooper PH, Mayer P, Baggiolini M. Stimulation of phagocytosis in bone marrow-derived mouse macrophages by bacterial lipopolysaccharide: correlation with biochemical and functional parameters. *J Immunol*. 1984;133:913-922.
30. Farbehi N, Patrick R, Dorison A, et al. Single-cell expression profiling reveals dynamic flux of cardiac stromal, vascular and immune cells in health and injury. *eLife*. 2019;8:1-39.
31. Ross J, Kongo M. The role of hypertrophy and growth factors in heart failure. *J Card Fail*. 1996;2:S121-S128.
32. Seropian IM, Toldo S, Van Tassell BW, Abbate A. Anti-inflammatory strategies for ventricular remodeling following St-segment elevation acute myocardial infarction. *J Am Coll Cardiol*. 2014;63:1593-1603.
33. Frangogiannis NG. The extracellular matrix in myocardial injury, repair, and remodeling. *J Clin Invest*. 2017;127:1600-1612.
34. Al-Khatib SM, Allen LaPointe NM, Kramer JM, Califf RM. What clinicians should know about the QT interval. *JAMA*. 2003;289:2120-2127.
35. Ricketts TD, Prieto-Dominguez N, Gowda PS, Ubil E. Mechanisms of macrophage plasticity in the tumor environment: manipulating activation state to improve outcomes. *Front Immunol*. 2021;12:1-20.
36. Frodermann V, Nahrendorf M. Macrophages and cardiovascular health. *Physiol Rev*. 2018;98:2523-2569.
37. Talman V, Ruskoaho H. Cardiac fibrosis in myocardial infarction—from repair and remodeling to regeneration. *Cell Tissue Res*. 2016;365:563-581.
38. Yoo W, Lee J, Noh KH, et al. Progranulin attenuates liver fibrosis by downregulating the inflammatory response. *Cell Death Dis*. 2019;10:758.
39. Fu X, Khalil H, Kanisicak O, et al. Specialized fibroblast differentiated states underlie scar formation in the infarcted mouse heart. *J Clin Invest*. 2018;128:2127-2143.
40. Zhu Y, Ohama T, Kawase R, et al. Progranulin deficiency leads to enhanced age-related cardiac hypertrophy through complement C1q-induced β-catenin activation. *J Mol Cell Cardiol*. 2020;138:197-211.
41. Nahrendorf M, Swirski FK. Monocyte and macrophage heterogeneity in the heart. *Circ Res*. 2013;112:1624-1633.
42. Hulsmans M, Sam F, Nahrendorf M. Monocyte and macrophage contributions to cardiac remodeling. *J Mol Cell Cardiol*. 2016;93:149-155.
43. Duncan SE, Gao S, Sarhene M, et al. Macrophage activities in myocardial infarction and heart failure. *Cardiol Res Pract*. 2020;2020:4375127.
44. Tarzami ST, Cheng R, Miao W, Kitsis RN, Berman JW. Chemokine expression in myocardial ischemia: MIP-2 dependent MCP-1 expression protects cardiomyocytes from cell death. *J Mol Cell Cardiol*. 2002;34:209-221.
45. Kao AW, Eisenhut RJ, Martens LH, et al. A neurodegenerative disease mutation that accelerates the clearance of apoptotic cells. *Proc Natl Acad Sci U S A*. 2011;108:4441-4446.
46. Matsumura SI, Iwanaga S, Mochizuki S, Okamoto H, Ogawa S, Okada Y. Targeted deletion or pharmacological inhibition of MMP-2 prevents cardiac rupture after myocardial infarction in mice. *J Clin Invest*. 2005;115:599-609.
47. Oishi Y, Spann NJ, Link VM, et al. SREBP1 contributes to resolution of pro-inflammatory TLR4 signaling by reprogramming fatty acid metabolism. *Cell Metab*. 2017;25:412-427.
48. Bystrom J, Evans I, Newson J, et al. Resolution-phase macrophages possess a unique inflammatory phenotype that is controlled by cAMP. *Blood*. 2008;112:4117-4127.
49. Shiraishi M, Shintani Y, Shintani Y, et al. Alternatively activated macrophages determine repair of the infarcted adult murine heart. *J Clin Invest*. 2016;126:2151-2166.
50. Wei F, Zhang Y, Jian J, et al. PGRN protects against colitis progression in mice in an IL-10 and TNFR2 dependent manner. *Sci Rep*. 2014;4:1-11.
51. Alexander AF, Kelsey I, Forbes H, Miller-Jensen K. Single-cell secretion analysis reveals a dual role for IL-10 in restraining and resolving the TLR4-induced inflammatory response. *Cell Rep*. 2021;36:109728.
52. Yang Q, Wang Y, Pei G, et al. Bone marrow-derived Ly6C− macrophages promote ischemia-induced chronic kidney disease. *Cell Death Dis*. 2019;10:291.
53. Frangogiannis NG, Dewald O, Xia Y, et al. Critical role of monocyte chemoattractant protein-1/CC chemokine ligand 2 in the pathogenesis of ischemic cardiomyopathy. *Circulation*. 2007;115:584-592.

SUPPORTING INFORMATION

Additional supporting information can be found online in the Supporting Information section at the end of this article.

How to cite this article: Sasaki T, Kuse Y, Nakamura S, Shimazawa M, Hara H. Progranulin deficiency exacerbates cardiac remodeling after myocardial infarction. *FASEB BioAdvances*. 2023;5:395-411. doi:10.1096/fba.2023-00084